

A Density-Functional Benchmark of Vibrational Free-Energy Corrections for Molecular Crystal Polymorphism

Joseph A. Weatherby,¹ Adrian F. Rumson,¹ Alastair J. A. Price,¹ Alberto Otero de la Roza,^{2, a)} and Erin R. Johnson^{1, 3, b)}

¹⁾*Department of Chemistry, Dalhousie University, 6274 Coburg Rd, Halifax, Nova Scotia, B3H 4R2, Canada*

²⁾*Departamento de Química Física y Analítica and MALTA Consolider Team, Facultad de Química, Universidad de Oviedo, 33006 Oviedo, Spain*

³⁾*Department of Physics and Atmospheric Science, Dalhousie University, 6310 Coburg Rd, Halifax, Nova Scotia, B3H 4R2, Canada*

(Dated: 21 February 2022)

Many crystal structure prediction protocols only concern themselves with the electronic energy of molecular crystals. However, vibrational contributions to the free energy (F_{vib}) can be significant in determining accurate stability rankings for crystal candidates. While force-field studies have been conducted to gauge the magnitude of these free-energy corrections, highly accurate results from quantum mechanical methods, such as density-functional theory (DFT), are desirable. Here, we introduce the PV17 set of 17 polymorphic pairs of organic molecular crystals, for which plane-wave DFT is used to calculate the vibrational free energies and free-energy differences (ΔF_{vib}) between each pair. Our DFT results confirm that the vibrational free-energy corrections are small, having a mean value of 1.0 kJ/mol and a maximum value of 2.3 kJ/mol for the PV17 set. Furthermore, we assess the accuracy of a series of lower-cost DFT, semi-empirical, and force-field models for computing ΔF_{vib} that have been proposed in the literature. It is found that calculating the F_{vib} using the Γ -point frequencies does not provide ΔF_{vib} values of sufficiently high quality. In addition, ΔF_{vib} values calculated using the various approximate methods have mean absolute errors relative to our converged DFT results of equivalent or larger magnitude than the vibrational free-energy corrections themselves. Thus, we conclude that, in a crystal structure prediction protocol, it is preferable to forego the inclusion of vibrational free energy corrections than to estimate them with any of the approximate methods considered here.

I. INTRODUCTION

Polymorphism,¹⁻³ the ability of a substance to exist in more than one crystalline phase, is of great interest in many domains of chemistry and materials science, particularly in drug development.^{4,5} Because polymorphs exhibit different chemical and physical properties, it is often interesting to know *a priori* whether a polymorph with certain desirable properties will be obtained. The field of molecular crystal-structure prediction (CSP)^{6,7} aims to use computational methods to predict the thermodynamically stable polymorph, which is often (but not necessarily) also the experimentally observed structure, beginning from the molecular diagram alone. CSP is particularly useful for the elucidation of crystal structures of new molecules, such as a pharmaceutical compound, or when searching for solid-state structures that exhibit specific properties like charge-carrier mobilities.^{8,9}

There is not one unique way to conduct a CSP study. The challenge is in determining a suitable balance between cost and accuracy to predict the likely isolable polymorph(s) and the crystal energy landscape. Candidate structures are initially generated by sampling the conformational and solid-form configuration space (usually with restrictions to the most common space

groups) of a molecule of interest.^{10,11} While dispersion-corrected density-functional theory (DFT) has shown promise for the subsequent energy ranking,¹²⁻²⁰ it still remains unfeasible to apply DFT to all candidates due to the vast number of structures generated. As a result, CSP studies tend to take the form of a multi-level refinement approach, where several methods are used sequentially to narrow the list of potential candidate structures.^{14,20-22} Classical force fields,²³ density-functional tight binding,^{24,25} or minimal-basis semi-empirical methods^{26,27} may be employed in the early stages of energy ranking to minimize the number of DFT calculations that need to be performed.

While there are notable exceptions,¹⁵⁻¹⁷ most CSP protocols are zeroth-order CSP,⁶ in which only the electronic energies are considered while other contributions to the free energy are neglected. In real molecular crystals, lattice vibrations, known as phonons, contribute in a small but significant way to the free energy. Using a classical force-field approach, it has been shown that the vibrational contributions to the free-energy difference for most organic polymorph pairs are quite small, rarely exceeding 2 kJ/mol.²⁸ Inclusion of vibrational effects still resulted in the reordering of ca. 10-20% of the studied structure pairs,^{28,29} due to the small energy differences between isolable polymorphs. Therefore, an accurate treatment of these vibrational effects is desirable in order to accurately determine the free-energy landscape of a given compound and to find the thermodynamically stable structure. However, due to the expensive nature

^{a)}Electronic mail: aoterodelaroz@gmail.com

^{b)}Electronic mail: erin.johnson@dal.ca

of phonon frequency calculations, it is at present very computationally demanding to use DFT methods to calculate vibrational free-energy corrections, especially for the large-unit-cell molecular crystals commonly encountered in CSP studies.

As an alternative, approximate methods and models have been proposed to compute the phonon frequencies and vibrational free-energy contributions at reduced cost. When using approximate methods, it is important to consider the trade-off between accuracy and cost. The vibrational free energies calculated using some approximate methods have been compared to converged DFT free energies for a few small molecular crystals.^{30–32} However, in CSP studies, we are interested in computing the relative free-energy corrections for a crystal structure pair, which may or may not benefit from error cancellation. In this work we propose a new benchmark set, termed the PV17 dataset, for vibrational free energies and energy differences of molecular crystals. The purpose of this new data set is twofold: i) to provide a reasonably sized benchmark set of high quality (harmonic) vibrational free energy data, and ii) because the dataset contains crystal pairs, it also allows the assessment of approximate methods regarding the calculation of vibrational free-energy differences, and consequently their suitability for incorporation into a CSP protocol.

To build the PV17 dataset, we use the Nyman polymorph library (NPL2016),²⁹ which contains a large set of molecular crystal structures primarily consisting of two polymorphs for a given organic molecule. A subset of 17 polymorph pairs from this library are identified involving crystals with small unit cells to ensure that the high-level benchmark calculations are feasible. The reference vibrational free-energy data in the PV17 dataset uses dispersion-corrected DFT to evaluate the phonon frequencies and vibrational free-energy corrections within the harmonic approximation. A fully anharmonic or even quasi-harmonic treatment would be desirable, but much more costly, and would complicate the application of the PV17 set to gauge the quality of approximate vibrational models. The B86bPBE-XDM^{33–35} functional is used in conjunction with a plane-wave basis set as our high-level method to calculate the reference vibrational free energies because of its high accuracy and reliability for molecular crystals.^{8,9,18,19,36}

Several approximate methods and models are examined in this work using the data in the new PV17 dataset: (i) distributed multipole analysis (DMA) force fields implemented in the DMACRYS package²³ using the Williams and FIT potentials; (ii) sHF-3c,^{26,27} which is a minimal-basis Hartree–Fock method with added empirical corrections for dispersion and basis-set incompleteness; and (iii) DFTB3-D3(BJ),²⁴ a dispersion-corrected density-functional tight-binding scheme. In addition, we also examine a recent pairing of DFTB3-D3(BJ) with a corrective model, termed the mode-matching³² approach, which has shown excellent results for computing various thermodynamic quantities. Mode matching serves as an

additive correction to the DFTB3-D3(BJ) phonon density of states, although it is easily applicable to other methods.

Our results confirm^{28,30,32} that computing vibrational corrections at the Γ -point only is insufficient to obtain converged values with both high and low levels of theory. The errors yielded by the approximate methods in the calculation of vibrational free-energy differences, including the mode-matching approach, are found to be comparable in magnitude to the free-energy differences themselves. This indicates that there are no grounds for preferring these approximate methods over zeroth-order CSP, and that further efforts are needed to develop accurate and cheap vibrational models for routine application in CSP studies. Overall, the converged vibrational corrections to the free-energy differences have values of 2.3 kJ/mol or less, with an average value of 1.0 kJ/mol, confirming the previous force-field result²⁸ that such corrections need only be applied when two (or more) candidate structures are nearly degenerate.

II. BACKGROUND THEORY

A. Phonons and free-energy corrections

Phonon frequencies (ω) are obtained at an arbitrary wavevector \mathbf{q} within the first Brillouin zone as solutions of the secular equation

$$\det \left| \frac{1}{\sqrt{M_m M_n}} \tilde{C}_{mn}^{\xi\eta}(\mathbf{q}) - \omega^2(\mathbf{q}) \right| = 0, \quad (1)$$

where M_m is the mass of atom m , ξ and η are the Cartesian directions, and \tilde{C} is the Fourier transform of the force-constant matrix, which is given by

$$C_{mn}^{\xi\eta} \equiv \frac{\partial^2 E}{\partial u_m^\xi \partial u_n^\eta}, \quad (2)$$

where u_m^ξ is the displacement of atom m in Cartesian direction ξ . The force-constant matrix is constructed as the second derivative of the potential-energy surface with respect to two nuclear displacements and can be computed via finite-difference methods or density-functional perturbation theory (DFPT).³⁷

Within the harmonic approximation, the Gibbs free energy is

$$G = E_{\text{static}} + F_{\text{vib}} + pV, \quad (3)$$

where E_{static} is the equilibrium, ground-state DFT energy, F_{vib} is the vibrational contribution to the Helmholtz free energy, and pV is the pressure-volume work, which is negligible at ambient pressure. The accurate calculation of F_{vib} and its difference between crystal pairs is the focus of this work. In the harmonic approximation, the vibrational free energy per unit cell can be computed

from the harmonic phonon frequencies as

$$F_{\text{vib}} = \frac{1}{N_{\mathbf{q}}} \sum_{i=1}^{3n} \sum_{\mathbf{q}} \frac{\hbar\omega_{i,\mathbf{q}}}{2} + k_B T \ln \left[1 - \exp \left(-\frac{\hbar\omega_{i,\mathbf{q}}}{k_B T} \right) \right], \quad (4)$$

where k_B is Boltzmann's constant and T is the temperature. The sums run over the $3n$ phonon branches (n is the number of atoms in the unit cell) and the $N_{\mathbf{q}}$ sampled \mathbf{q} -points in the first Brillouin zone. The first term in Eq. 4 is the zero-point energy and the second is the temperature-dependent contribution to the F_{vib} .

In this work, the finite-difference approach is used to calculate the force-constant matrix (Eq. 2). The convergence of the F_{vib} with respect to the size of the supercell or, equivalently, the \mathbf{q} -point sampling of the Brillouin zone, was studied by systematically varying the supercell according to the formula

$$n_i = \text{int} \left[\max \left(1, R_k |b_i| + \frac{1}{2} \right) \right], \quad (5)$$

where n_i is the size of the supercell in the $i = a, b$, and c directions, b_i is the corresponding reciprocal lattice vector of the primitive unit cell, and R_k is a length parameter. For each individual crystal, the R_k parameter was increased until the F_{vib} was converged to within a threshold of 0.5 kJ/mol per molecule. The phonon frequencies were then Fourier-reinterpolated on a $12 \times 12 \times 12$ Monkhorst-Pack³⁸ mesh, and the final value of F_{vib} was calculated by integration. An example of the difference between the converged phonon density of states (phDOS) and one obtained by reinterpolation using only the Γ -point is shown in Figure 1 for the $I\beta$ phase of ethylenediamine. It is clear from this figure that sampling \mathbf{q} points other than Γ is essential to capture the features of the phDOS, particularly at low frequency. It is important to note that the second, temperature-dependent, term in the harmonic free energy (Eq. 4) diverges when $\omega \rightarrow 0$. Therefore, the low-frequency region of the phDOS dominates the thermal contribution to the harmonic free energy, for which reason it is essential to model the dispersion of the low-frequency vibrations correctly.

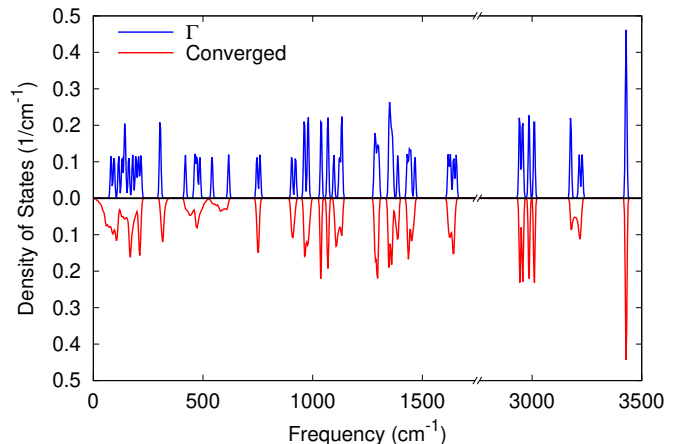
B. Mode Matching

The mode matching method is a hybrid approximate model recently proposed by Cook and Beran designed to correct the low-level DFTB3-D3(BJ) phonon density of states to yield accurate thermodynamic properties in molecular crystals.³² The mode matching approach calculates the harmonic vibrational frequency for mode i at point \mathbf{q} , $\omega_i(\mathbf{q})$, as

$$\omega_i(\mathbf{q}) \approx \omega_i^{\text{low}}(\mathbf{q}) + \left[\omega_i^{\text{high}}(\Gamma) - \omega_i^{\text{low}}(\Gamma) \right]. \quad (6)$$

There are three items required for the evaluation of the mode matching frequencies: i) phonon frequencies

FIG. 1. Overlay of the DFT phDOS for the $I\beta$ phase of ethylenediamine (CCDC code ETDIAM16) computed at Γ and using a converged \mathbf{q} -point grid.



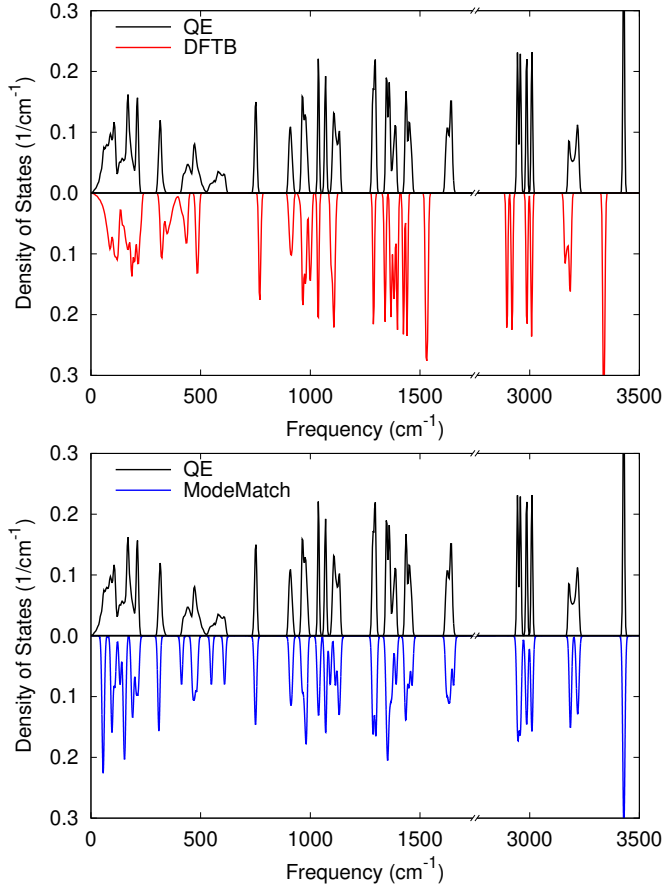
at Γ computed with an accurate high-level theoretical method, ii) the frequencies at Γ calculated with a cheaper, less accurate, low-level method, and iii) the converged phDOS from the less accurate method. In Cook and Beran's work, plane-wave DFT was employed for the high level of theory and DFTB for the low level method. An example of mode matching is shown in Figure 2 for the $I\beta$ phase of ethylenediamine. The advantage of this simple model is that it is no longer necessary to adequately sample the Brillouin zone with DFT, and instead DFTB can be used for this purpose, which leads to a significant reduction in computational cost. Figure 2 shows that the mode matching method is successful in reproducing the high-frequency, low-dispersion features of the phDOS. However, the low-frequency acoustic part of the phDOS as well as the region encompassing the intermolecular lattice vibrations, which dominate the thermal contribution to the free energy, are not as well reproduced.

C. Treatment of the Acoustic Modes

Acoustic phonons correspond to low-frequency long-wavelength vibrations of the solid and, hence, are the slowest to converge with respect to \mathbf{q} -point sampling. Due to their low frequencies, the acoustic modes (AM) also have high contributions to the temperature-dependent term of the F_{vib} (Eqn. 4). In addition, due to the fact that the acoustic frequencies at Gamma are not zero, Cook and Beran's mode matching method cannot be applied to correct the DFTB acoustic frequencies using the DFT frequencies at Γ .

One way of evaluating the acoustic contribution to the F_{vib} is the Debye model, in which the solid is assumed to behave like a vibrating continuum and the acoustic vibrations are treated as stationary waves spanning the whole crystal. A slightly different version of the Debye model

FIG. 2. Top: Overlay of the phDOS of the $I\beta$ phase of ethylenediamine (ETDIAM16) computed with QE and DFTB using a converged supercell. Bottom: the same phDOS with QE and the shifted DFTB phDOS calculated using the mode matching method.



was proposed by Nyman et al.³⁰ and subsequently used by Cook and Beran³² to treat the vibrational acoustic modes (AM). In this AM model, the phonon dispersion is assumed to be sinusoidal in the wave-vector, as in a one-dimensional atom chain. The acoustic frequencies are given in terms of a Debye-like frequency, ω_D , by

$$\omega_{ac} = \omega_D \sin\left(\frac{\pi}{2} \frac{|\mathbf{q}|}{|\mathbf{q}_{zb}|}\right), \quad (7)$$

where $|\mathbf{q}_{zb}|$ is the norm of the vector \mathbf{q} at the corresponding Brillouin zone boundary. The Debye-like frequency

$$\omega_D = \frac{2v|\mathbf{q}_{zb}|}{\pi}, \quad (8)$$

is therefore the frequency at the zone boundary for the corresponding direction in reciprocal space (consider $\mathbf{q} = \mathbf{q}_{zb}$ in Eq. 7). In this equation, v is the velocity of sound propagating through the crystal along direction \mathbf{q} obtained by solving the Christoffel equation,

$$\det[\Gamma_{ij} - \rho v^2 \delta_{ij}] = 0, \quad (9)$$

where ρ is the density and δ_{ij} is the Kronecker delta. The Γ_{ij} 's are the 3×3 Christoffel matrices given by

$$\Gamma_{ij} = \sum_{nm} \mathbf{q}_n C_{inmj} \mathbf{q}_m, \quad (10)$$

where \mathbf{q}_n are direction vector Cartesian components in reciprocal space.

In their AM model, Nyman et al. chose 13 symmetry-unique directions, corresponding to the simplest Lebedev integration quadrature, and used them to compute an average Debye frequency, which is ultimately the only parameter in the model.^{30,32} The elastic constant tensor (C_{inmj}) required to calculate the sound velocities along the different propagation directions is computed using the stress-strain relations. DFT calculations for a series of small unit-cell deformations at the equilibrium geometry are used to determine the stress as a function of strain and linear least-squares fits are used to compute the elastic constant tensor.³²

III. COMPUTATIONAL METHODOLOGY

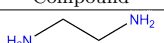
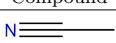
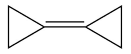
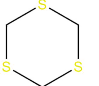
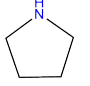
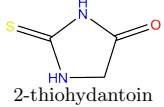
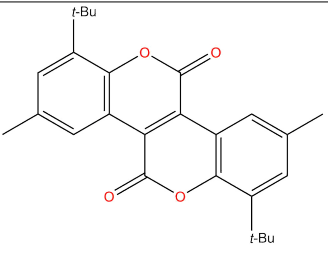
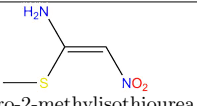
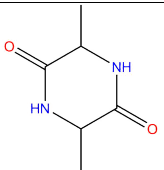
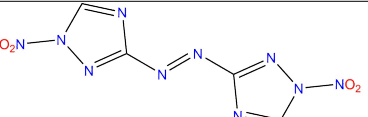
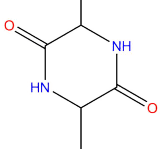
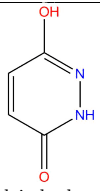
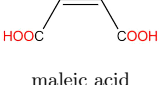
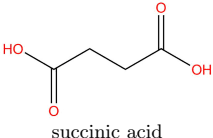
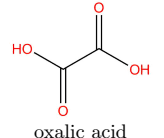
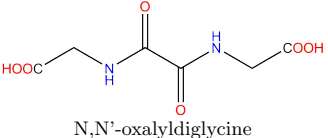
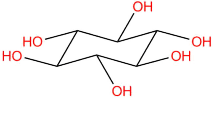
Geometry optimization and phonon frequency calculations were performed for our benchmark set of polymorph pairs in order to calculate the harmonic F_{vib} . In all geometry optimizations, both the atomic positions and lattice vectors were allowed to fully relax, unless otherwise specified. Phonons were always calculated at the same level of theory as the geometry optimization. All free energies were calculated at 300 K. The specific parameters used within each method are given below.

Phonon frequency calculations conducted with the Quantum ESPRESSO,³⁹ CRYSTAL17,⁴⁰ and DFTB+²⁴ packages used the frozen phonon method as implemented in the `phonopy`⁴¹ code, v. 2.9.3. The mode matching calculations used the `Modematch` program of Ref. 32. The force-field calculations used the `DMACRYS`²³ code, v. 2.3.0, together with the `autold` and `autofree` programs of Nyman,²⁹ which construct a series of linear supercells required to obtain the phonons beyond the Γ -point and subsequently calculate the vibrational free energy.

Plane-wave DFT⁴³ calculations used periodic boundary conditions and the projector augmented-wave (PAW)⁴⁴ approach implemented in the Quantum ESPRESSO³⁹ (QE) software package, v. 6.5. We used the B86bPBE^{33,34} generalized-gradient approximation functional and the exchange-hole dipole moment (XDM) dispersion model.^{35,45} The convergence thresholds were set to 10^{-5} and 10^{-4} Ry for the energy and forces, respectively. In addition, the convergence in the pressure was set to 10^{-2} kbar. Kinetic-energy and charge-density cutoffs of 80 Ry and 800 Ry, respectively were used along with a Monkhorst-Pack (MP)³⁸ \mathbf{k} -point mesh selected by using an R_k value of 50 bohr in Eq. 5.

sHF-3c^{26,27} calculations were performed using the CRYSTAL17⁴⁰ code. Full geometry optimizations (cell and atomic positions) were carried out starting from

TABLE I. Molecular structures, Cambridge Crystallographic Data Centre (CCDC)⁴² codes, converged B86bPBE-XDM F_{vib} values (in kJ/mol per molecule), and the corresponding supercell sizes, for all crystal structures in the PV17 dataset.

Compound	CSD code	Supercell	F_{vib}	Compound	CSD code	Supercell	F_{vib}
 ethylenediamine	ETDIAM16 ETDIAM18	2×1×2 2×2×1	274.77 276.21	 acetonitrile	QQQCIV01 QQQCIV08	3×1×2 3×3×1	105.55 106.45
 bicyclopropylidene	CUMMIG01 CUMMIG02	2×1×3 2×3×2	286.26 285.07	 1,3,5-trithiane	TRITAN03 TRITAN10	2×2×1 2×2×2	201.79 201.95
 pyrrolidine	EFUMAU EFUMAU03	2×2×1 2×3×1	315.50 315.20	 2-thiohydantoin	THHYDT THHYDT02	3×2×2 3×2×1	184.47 183.45
 1,7-di- <i>t</i> -butyl-3,9-dimethyl-dibenzonaphthyrone	DAVVUR DAVVUR	1×2×2 1×2×2	1163.31 1163.31	 1-nitro-2-methylisothiourea	XOCJEE XOCJEE01	2×1×4 2×2×2	209.12 207.39
 cyclo-D-alanyl-L-alanyl	TRDMPP01 TRDMPP02	2×2×2 1×2×2	400.69 402.83	 1,1'-dinitro-3,3'-azo-1,2,4-triazole	GICTIV GICTIV01	2×1×2 2×2×1	242.64 242.90
 maleic acid	MALIAC12 MALIAC13	2×1×2 4×2×1	190.94 190.81	 maleic hydrazide	MALEHY10 MALEHY12	2×2×2 3×2×2	204.85 205.05
 fumaric acid	FUMAAC FUMAAC01	2×1×2 3×2×2	191.14 193.02	 succinic acid	SUCACB02 SUCACB07	2×1×2 2×2×3	251.65 250.32
 oxalic acid	OXALAC03 OXALAC04	2×1×2 2×1×2	113.07 111.49	 N,N'-oxalyldiglycine	REKBUE REKBUE01	3×2×1 3×3×1	379.18 378.73
 scyllo-inositol	EFURIH EFURIH04	2×2×1 2×2×2	489.43 489.03				

the B86bPBE-XDM equilibrium geometries. The convergence thresholds on the root-mean-square in the gradient and displacement between subsequent optimization steps were set to 3×10^{-5} and 1.2×10^{-4} a.u., respectively, which are one order of magnitude smaller than the default values. The maximum value for the trust radius was set to 0.25 a.u. and a $4 \times 4 \times 4$ MP \mathbf{k} -point mesh was used. Phonon frequencies were scaled by 0.86, as recommended by Ref. 26.

SCC-DFTB3-D3(BJ)^{24,25} calculations with the 3ob-3-1²⁵ parametrization were performed using the DFTB+²⁴ code, v. 20.2.1. Full geometry optimizations were started from the QE equilibrium geometries. The

MaxForceComponent parameter, which sets the threshold for convergence in the forces, was set to 10^{-5} a.u. Atomic Hubbard derivatives and the parameters used in the D3(BJ) dispersion model were set to those described in Ref. 25.

Force-field calculations were carried out under the rigid-body approximation as implemented in the DMACRYS²³ code, which employs distributed atomic multipoles to represent electrostatic contributions. Both the FIT⁴⁶ and the Williams (W99)⁴⁷ force fields were used, where W99 was supplemented with parameters for sulfur from Ref. 48. Atom-centered multipoles were calculated up to rank 4 (hexadecapole) from a distributed

multipole analysis⁴⁹ of the electronic density computed using B3LYP/6-31G** with the Gaussian09⁵⁰ program. Rigid-molecule lattice relaxations were then performed, followed by computation of the phonon frequencies⁵¹ using the `autold` and `autofree` programs of Nyman.³⁰ `autold` generates a series of linear supercells to sample the Brillouin zone beyond the Γ -point;³⁰ here we selected a target \mathbf{q} -point distance of 0.12 \AA^{-1} . `autofree` then collects the frequencies from the supercells and computes the F_{vib} .

IV. RESULTS

A. The PV17 Benchmark

The PV17 benchmark was assembled using the Nyman Polymorph Library²⁹ as a starting point. Structures in the library were sorted by cell volume, as this roughly correlates with the numbers of atoms and electrons within the unit cell, and with the computational cost of the eventual phonon frequency calculations. We selected polymorph pairs with both members having volumes less than 600 \AA^3 for further consideration. This choice is necessary to keep the cost of the DFT phonon calculations feasible, although it may introduce a bias in the benchmark set towards small and rigid molecules. We then proceeded to perform geometry relaxation and phonon calculations on this subset. Compounds were eliminated from the benchmark if convergence problems were encountered, if the supercell sizes required for the phonon calculations exceeded our available computational resources, or if both “polymorphs” converged to the same structure upon relaxation. This can occur if the two reference experimental crystal structures have essentially the same packing, but were determined at different temperatures.⁵²

The resulting benchmark set of 17 polymorph pairs is shown in Table I, along with the converged F_{vib} values and corresponding supercell sizes for each crystal. The final results for the ΔF_{vib} between each polymorph pair are shown in Table II. By convention, we take ΔF_{vib} as the F_{vib} value obtained for the structure with the higher number in its assigned CCDC code minus that for the structure with the lower numbered CCDC code.

In a previous study using a distributed-multipole force field approach, Nyman and Day²⁸ found the harmonic $|\Delta F_{\text{vib}}|$ to be less than 1 kJ/mol for more than 70% of the polymorph pairs studied in their work, and greater than 2 kJ/mol in fewer than 6% of cases. Table II shows a summary of our high-level B86bPBE-XDM results, giving the electronic energy difference between each polymorph pair, the converged ΔF_{vib} , and the resulting free-energy difference. Compared to Nyman and Day’s results, the DFT values are similar, although somewhat larger than the force-field results. The average $|\Delta F_{\text{vib}}|$ is 1 kJ/mol and values greater than 2 kJ/mol occur for 2/17 (12%) of the compounds considered, although no values exceeded 2.5 kJ/mol for our limited dataset. However, we

TABLE II. Computed B86bPBE-XDM relative electronic energies (ΔE), converged vibrational free-energy corrections (ΔF_{vib}), and relative free energies (ΔG), for the PV17 benchmark. All values are in units of kJ/mol per molecule. The last row shows the average magnitude of each quantity.

Polymorph Pair	ΔE	ΔF_{vib}	ΔG
ETDIAM	0.0	1.4	1.4
QQQCIV	-0.6	0.9	0.3
CUMMIG	4.9	-1.2	3.7
TRITAN	-0.3	0.2	-0.1
EFUMAU	1.0	-0.3	0.7
THHYDT	-1.2	-1.0	-2.2
DAVVUR	-4.6	2.3	-2.3
XOCJEE	0.8	-1.7	-0.9
GICTIV	-6.7	0.3	-6.5
TRDMPP	-2.0	2.1	0.1
MALEHY	-0.2	0.2	0.0
MALIAC	0.3	-0.1	0.2
FUMAAC	-7.4	1.9	-5.5
OXALAC	-2.4	-1.6	-4.0
SUCACB	0.0	-1.3	-1.4
REKBUE	-3.5	-0.5	-4.0
EFURIH	-6.0	-0.4	-6.4
Avg.	2.5	1.0	2.3

expect greater differences in the optical region of the ph-DOS, and therefore greater $|\Delta F_{\text{vib}}|$, if the molecules under study are larger and more flexible than those present in the PV17 set, particularly if polymorphs present different molecular conformations.

Nyman and Day also determined that vibrational free-energy corrections altered the stability ordering for roughly 9% of polymorph pairs when employing the harmonic approximation.²⁸ Our results in Table II show that the ordering is reversed for 3/17 pairs (18%). There were a further two pairs that were predicted to be degenerate based on the electronic energy alone, for which the F_{vib} entirely determines the stability ranking.

Lastly, the results in Table II suggest that the accuracy requirement for the adequate calculation of ΔF_{vib} between polymorph pairs is quite high. For instance, the best available DFT-based multilevel methods for the calculation of host-guest binding energies yield association free energies with an average error above 2 kcal/mol (8.4 kJ/mol).⁵³ The average ΔF_{vib} in Table II is 8 times lower than this value and, in fact, all our examined low-level methods (Table III) yield absolute F_{vib} for individual crystals with average errors lower than 2 kcal/mol.

B. Assessment of Low-Level Methods

With our benchmark values in hand, we proceed to assess the performance of selected low-cost methods for prediction of F_{vib} and ΔF_{vib} for our set of 17 polymorph pairs. The results are collected in Table III for F_{vib} and Table IV for ΔF_{vib} . Γ indicates results obtained using only the Γ point, while “Conv.” indicates results ob-

TABLE III. Absolute F_{vib} (kJ/mol per molecule) values for all crystals in our PV17 benchmark set. Results are shown for three electronic structure methods (sHF-3c, DFTB3-D3(BJ), and B86bPBE-XDM) and the mode-matching approach. Free energies were calculated using either the Γ point only or with a converged (Conv) supercell. For B86bPBE-XDM, results are also given for the combination of Γ -point frequencies for the optical and the AM model for the acoustic modes (Γ +AM).

Polymorph Pair	sHF-3c		DFTB3-D3(BJ)		Mode Match	B86bPBE-XDM		
	Γ	Conv	Γ	Conv		Γ	Γ +AM	Conv
ETDIAM16	285.5	281.5	275.8	272.3	273.6	279.3	274.3	274.8
ETDIAM18	287.1	282.4	275.8	272.6	275.1	280.7	275.7	276.2
QQQCIV01	108.6	106.0	107.4	105.1	104.7	107.9	105.0	105.5
QQQCIV08	109.0	106.3	110.7	107.3	105.7	110.3	105.9	106.4
CUMMIG01	297.0	293.4	289.5	287.8	286.5	289.5	283.8	286.3
CUMMIG02	297.6	293.5	289.1	287.5	283.8	288.5	281.7	285.1
TRITAN03	208.3	205.4	205.5	203.6	200.9	204.3	200.7	201.8
TRITAN10	210.9	204.9	207.2	203.2	201.0	207.3	200.8	202.0
EFUMAU	327.3	325.4	317.3	316.2	314.7	317.3	313.5	315.5
EFUMAU03	327.4	325.3	318.2	316.6	313.2	316.7	313.1	315.2
THHYDT	185.5	182.3	189.0	186.7	184.4	187.2	184.5	184.5
THHYDT02	185.7	179.7	189.7	185.6	181.9	188.4	182.1	183.4
DAVVUR	1198.5	1185.1	1182.5	1171.7	1159.0	1175.5	1160.9	1163.3
DAVVUR01	1202.7	1188.7	1187.4	1176.1	1161.8	1179.0	1163.8	1165.7
XOCJEE	208.8	204.0	214.9	212.1	205.9	212.4	205.7	209.1
XOCJEE01	208.6	203.2	212.7	208.7	206.1	212.6	206.0	207.4
GICTIV	231.8	227.2	260.1	258.4	240.3	243.3	236.5	242.6
GICTIV01	234.6	227.3	267.7	265.1	238.7	247.8	238.7	242.9
TRDMPP01	405.8	399.9	404.4	399.8	399.6	406.2	399.8	400.7
TRDMPP02	409.1	404.0	403.9	399.6	400.4	407.0	400.0	402.8
MALEHY10	208.8	205.0	211.1	207.4	203.5	209.5	203.6	204.8
MALEHY12	205.5	203.2	207.3	207.1	204.0	206.1	202.1	205.1
MALIAC12	189.8	187.8	192.4	192.0	190.0	192.6	189.3	190.9
MALIAC13	193.1	187.6	194.2	189.9	189.4	194.8	189.0	190.8
FUMAAC	187.0	185.7	192.3	191.6	188.3	191.3	187.4	191.1
FUMAAC01	197.3	188.9	198.9	193.3	189.9	200.6	190.0	193.0
OXALAC03	109.8	107.6	113.4	111.5	111.8	114.9	111.8	113.1
OXALAC04	111.0	107.6	113.9	111.7	110.3	114.5	109.4	111.5
SUCACB02	255.6	250.9	254.9	253.0	250.8	255.2	250.0	251.6
SUCACB07	253.5	249.0	253.1	250.2	248.1	253.8	247.5	250.3
REKBUE	376.3	370.1	379.9	375.1	377.9	384.6	378.3	379.2
REKBUE01	381.1	371.3	381.4	375.5	376.9	387.8	375.7	378.7
EFURIH	497.8	494.4	479.9	476.9	488.0	492.9	487.3	489.4
EFURIH04	498.0	493.4	479.5	475.1	486.5	493.6	487.1	489.0
MAE	7.3	6.0	5.6	3.8	1.7	4.2	2.0	-
MAX	37.1	23.0	24.8	22.2	4.4	13.3	6.1	-

tained using a converged supercell. Specific to the plane-wave DFT data, we also include the free-energy results calculated using the Γ -point frequencies for the optical contribution and the AM model for the acoustic contribution, as this is much more computationally expedient than fully converging the F_{vib} . These latter results allow us to determine the relative importance of converging the optical and acoustic modes for computation of ΔF_{vib} .

Considering the absolute F_{vib} values in Table III, Γ -point-only calculations give fairly large errors, following the order of HF-3c>DFTB+>DFT. In contrast, using the AM model for the acoustic contribution and calculating the optical contribution to the free energy with the DFT Γ -point frequencies results in quite good performance, with a mean absolute error (MAE) of only 2.0 kJ/mol. This error can be reduced even further, to 1.7 kJ/mol, by accounting for \mathbf{q} -point dependence of

the optical modes using a converged DFTB calculation in combination with the mode matching approach. This confirms the high accuracy of the mode matching method seen for F_{vib} in Cook and Beran’s study.³²

Table IV compares the performance of the various examined methods in the calculation of vibrational free energy differences for polymorph pairs. In this table and unlike Table III, we have also included DMACRYS results with the FIT and W99 force fields. The reason for this difference is that, because the DMA force fields use rigid molecules, it is not possible to calculate the intramolecular contribution to F_{vib} . The DMA force field results in Table IV assume implicitly that the intramolecular contribution to the vibrational free energy is the same for both polymorphs.

In contrast to the results for the absolute free energies, we no longer see significant differences in performance

TABLE IV. Relative F_{vib} (kJ/mol per molecule) values for all polymorph pairs in the PV17 benchmark set. Results are shown for two DMA force fields (DMACRYS), three electronic structure methods (sHF-3c, DFTB3-D3(BJ), and B86bPBE-XDM), and the mode-matching approach. Results are reported using either the Γ point or with a converged (Conv) supercell. Only converged results are shown for the DMA calculations. For B86bPBE-XDM, results are also given using the Γ point with the AM correction (Γ +AM).

Polymorph Pair	DMACRYS		sHF-3c		DFTB3-D3(BJ)		Mode Match	B86bPBE-XDM		
	W99	FIT	Γ	Conv	Γ	Conv		Γ	Γ +AM	Conv
ETDIAM	0.0	0.5	1.6	0.9	0.1	0.2	1.4	1.4	1.4	1.4
QQQCIV	0.3	0.3	0.4	0.3	3.3	2.2	1.0	2.3	0.9	0.9
CUMMIG	0.3	0.5	0.7	0.1	-0.4	-0.3	-2.7	-1.0	-2.1	-1.2
TRITAN	1.4	-0.1	2.6	-0.5	1.7	-0.5	0.1	3.1	0.1	0.2
EFUMAU	0.6	0.3	0.1	0.0	0.9	0.4	-1.5	-0.6	-0.4	-0.3
THHYDT	0.5	0.7	0.2	-2.6	0.6	-1.1	-2.5	0.8	-2.4	-1.0
DAVVUR	1.1	1.1	4.2	3.6	4.9	4.4	2.8	3.4	2.9	2.3
XOCJEE	-0.4	-0.3	-0.3	-0.8	-2.2	-3.4	0.2	0.2	0.3	-1.7
GICTIV	0.3	0.7	2.8	0.1	7.6	6.7	-1.6	4.5	2.2	0.3
TRDMPP	1.4	1.3	3.3	4.1	-0.4	-0.1	0.8	0.8	0.2	2.1
MALEHY	-1.4	-1.6	-3.3	-1.8	-3.8	-0.2	0.5	-3.3	-1.5	0.2
MALIAC	-0.1	-0.2	3.2	-0.2	1.7	-2.0	-0.6	2.3	-0.3	-0.1
FUMAAC	2.0	2.2	10.3	3.2	6.5	1.8	1.6	9.3	2.6	1.9
OXALAC	0.7	-0.2	1.3	0.0	0.5	0.1	-1.5	-0.4	-2.4	-1.6
SUCACB	-0.7	-1.6	-2.0	-1.9	-1.8	-2.8	-2.8	-1.5	-2.5	-1.3
REKBUE	0.8	-0.4	4.9	1.2	1.5	0.4	-1.0	3.3	-2.6	-0.5
EFURIH	0.9	-0.7	0.2	-1.1	-0.4	-1.7	-1.5	0.8	-0.2	-0.4
MAE	1.1	0.8	2.2	1.0	2.1	1.5	0.8	2.0	0.9	-
MAX	2.3	1.8	8.4	2.0	7.3	6.4	1.9	7.4	2.2	-

between the three QM methods when considering free-energy differences. Γ -point only calculations with sHF-3c, DFTB3-D3(BJ), and B86bPBE-XDM all yield mean absolute errors (MAEs) of nearly 2 kJ/mol and maximum errors (MAX) of 7.3-8.4 kJ/mol. In some cases, most notably for fumaric acid (FUMAAC), the ΔF_{vib} computed using only the Γ point can be much higher than the converged values, emphasizing the importance of properly accounting for the low-frequency phonon dispersion and the acoustic contributions. Thus, using only the Γ -point frequencies to assess the magnitude of the free-energy correction in CSP studies may be quite misleading, and is not recommended.

Comparing the force-field, converged low-level QM, and mode matching results with the converged B86bPBE-XDM reference values, we see that all give fairly equivalent error statistics, with MAEs of 0.8-1.5 kJ/mol and maximum errors of ca. 2-7 kJ/mol. Of these approaches, DFTB3-D3(BJ) gives the largest error for 1,1'-dinitro-3,3'-azo-1,2,4-triazole (GICTIV), indicating that it might not perform well for azo compounds. Indeed, from Table III, GICTIV shows the largest errors in absolute F_{vib} for DFTB3-D3(BJ) as well. Mode matching tends to give lower errors than the converged DFTB results, particularly for acetonitrile (QQQCIV), 1,7-di-*t*-butyl-3,9-dimethyl-dibenzonaphthyrone (DAVVUR), 1,1'-dinitro-3,3'-azo-1,2,4-triazole (GICTIV), and most of the systems with dimeric H-bonds involving either COOH or CONH groups. However, it is notable that the DMA force fields give comparable overall errors to the semi-empirical QM

methods, and mode matching, with a much lower computational cost.

Finally, we consider the performance of using the B86bPBE-XDM optical contribution estimated from the Γ -point frequencies coupled with AM model for the acoustic contribution. The rationale beyond this combination is that the low-frequency, long-wavelength acoustic modes are the slowest to converge with respect to \mathbf{q} -points and are missing from the Γ -point treatment entirely. We can therefore add the acoustic contribution to F_{vib} from the approximate AM model to the Γ -point results as a correction and, because the optical modes typically have a weaker dependence on \mathbf{q} -points, this may be a good approximation to the converged result. The AM approximation has an additional set of calculations on top of the Γ -point frequency calculations, since it requires evaluation of the elastic constants.

Inclusion of the AM model correction more than halves the MAE relative to the Γ -point-only results with B86bPBE-XDM. Notably the Γ +AM approach gives significantly better agreement with the converged reference values for many of the polymorph pairs, such as acetonitrile (QQQCIV), 1,3,5-trithiane (TRITAN), 1,1'-dinitro-3,3'-azo-1,2,4-triazole (GICTIV), maleic hydrazide (MALEHY), maleic acid (MALIAC), N,N'-oxalyldiglycine (REKBUE), and most significantly fumaric acid (FUMAAC), which consistently have the largest error in the Γ -point calculations. Once more, this result highlights the importance of properly accounting for the acoustic contributions to ΔF_{vib} .

The cases where Γ +AM still gives errors in ex-

cess of 1 kJ/mol are 2-thiohydantoin (THHYDT), 1,1'-dinitro-3,3'-azo-1,2,4-triazole (GICTIV), cyclo-D-alanyl-L-alanyl (TRDMPP), maleic hydrazide (MALEHY), succinic acid (SUCACB), and N,N'-oxalyldiglycine (REKBUE). With one exception, all of these compounds form dimeric H-bonds involving two COOH or CONH groups. This suggests that optical modes involving strong, cooperative H-bonding networks require more extensive \mathbf{q} -point sampling and that changes in these H-bonding motifs between polymorphs have significant contributions to ΔF_{vib} . The remaining errors in the Γ +Debye results may be due to either neglect of the dependence of the optical modes on \mathbf{q} -points, as seen for the dimeric H-bonds, or to breakdowns of the AM model approximation.

V. DISCUSSION AND CONCLUSIONS

This work presented the new PV17 benchmark, containing DFT absolute (F_{vib}) and relative (ΔF_{vib}) harmonic vibrational free energy data for pairs of crystalline organic polymorphs. This benchmark was used to assess the performance of several force-field and semi-empirical QM methods for prediction of relative free-energy corrections in molecular crystal polymorph pairs. Both plane-wave DFT frequency calculations at the Γ point, augmented with treatment of the acoustic modes using a Debye-like model, and the recent mode-matching approach³² showed good performance for prediction of the absolute F_{vib} for the individual molecular crystals.

However, none of the methods studied were able to benefit significantly from error cancellation in the evaluation of ΔF_{vib} for the polymorph pairs. Overall, the MAEs obtained with all examined methods were comparable to the average magnitude of ΔF_{vib} itself. As an illustration, a method that consistently gives a ΔF_{vib} of zero, which is equivalent to a zeroth-order CSP protocol, would yield an MAE of 1.0 kJ/mol and MAX error of 2.3 kJ/mol, which are on par with, or better than, the results obtained with all of the methods considered in this study. Thus, although free energies calculated at a low-level of theory may be useful in other contexts, our recommendation at present is to neglect thermal free-energy effects on CSP ranking entirely, rather than to calculate them with a low level of theory and introduce an additional uncontrolled error. However, some of the approaches examined, like Cook and Beran's mode matching approach and also combining a DFT Γ -point frequency calculation with a model for the acoustic contribution do show promise, but more work is required until practical CSP protocols can benefit from these methods.

While the magnitudes of our predicted thermal corrections were slightly larger than those obtained previously, we confirm the finding of Nyman and Day²⁸ that ΔF_{vib} is generally small in magnitude. This means that thermal effects need only be taken into account at the conclusion of a CSP protocol if two or more polymorphs are nearly degenerate, with a relative energy difference of less than

ca. 2.5 kJ/mol.

Calculating ΔF_{vib} for polymorph pairs is very challenging because it is a small difference between large numbers. The individual F_{vib} values have typical magnitudes of ca. 100-500 kJ/mol per molecule for the molecular crystals considered here, while the differences between polymorphs of the same compound have magnitudes under 2.5 kJ/mol. Thus, it is reasonable that converging the total F_{vib} to within 0.5 kJ/mol, which requires relatively dense \mathbf{q} -point grids in some cases, may not be entirely satisfactory for the purpose of CSP candidate ranking based on the free energy. In addition, we have not considered quasi-harmonic or anharmonic effects, whose inclusion would complicate matters even further. While the present work represents an advance over the previous assessment of ΔF_{vib} using DMA potentials, even more precise benchmarks for ΔF_{vib} are highly desirable, as well as the development of more accurate vibrational models for organic molecular crystals.

SUPPLEMENTARY MATERIAL

Crystal structures for all polymorphs in the PV17 benchmark, optimized with B86bPBE-XDM using Quantum ESPRESSO.

ACKNOWLEDGEMENTS

We thank Cameron Cook, Drs. Gregory Beran, Jonas Nyman, and Graeme Day for providing access to their `Modematch`, `autold`, and `autofree` programs. This research was funded by the Natural Sciences and Engineering Research Council of Canada (NSERC). The authors are grateful to Compute Canada for computational resources. We also thank the Government of Nova Scotia for a fellowship to JAW. AOR thanks the Spanish Ministerio de Ciencia e Innovación and the Agencia Estatal de Investigación (AEI) (project PGC2018-097520-A-100), the Principality of Asturias (FICYT) and FEDER (project AYUD/2021/51036), and the Spanish MINECO for a Ramón y Cajal fellowship (RyC-2016-20301).

DATA AVAILABILITY

The data that support the findings of this study are available within the article and its supplementary material.

REFERENCES

- ¹A. J. Cruz-Cabeza, N. Feeder, and R. J. Davey, *Commun. Chem.* **3**, 142 (2020).

- ²A. J. Cruz-Cabeza, S. M. Reutzel-Edens, and J. Bernstein, *Chem. Soc. Rev.* **44**, 8619 (2015).
- ³J. Bernstein, *Polymorphism in Molecular Crystals* (Oxford University Press, 2020).
- ⁴R. Hilfiker and M. von Raumer, *Polymorphism in the Pharmaceutical Industry: Solid Form and Drug Development* (John Wiley & Sons, 2018).
- ⁵D. Gentili, M. Gazzano, D. Jones, and M. Cavallini, *Chem. Soc. Rev.* **48**, 2502 (2019).
- ⁶S. L. Price, *Faraday Discuss.* **211**, 9 (2018).
- ⁷A. R. Oganov, *Faraday Discuss.* **211**, 643 (2018).
- ⁸Y. Yang, B. Rice, X. Shi, J. R. Brandt, R. Correa da Costa, G. J. Hedley, D.-M. Smilgies, J. M. Frost, I. D. W. Samuel, A. Otero-de-la-Roza, E. R. Johnson, K. E. Jelfs, J. Nelson, A. J. Campbell, and M. J. Fuchter, *ACS Nano* **11**, 8329 (2017).
- ⁹B. Rice, L. M. LeBlanc, A. Otero-de-la-Roza, M. J. Fuchter, E. R. Johnson, J. Nelson, and K. E. Jelfs, *Nanoscale* **10**, 1865 (2018).
- ¹⁰C. W. Glass, A. R. Oganov, and N. Hansen, *Comput. Phys. Commun.* **175**, 713 (2006).
- ¹¹Y. Wang, J. Lv, L. Zhu, and Y. Ma, *Comput. Phys. Commun.* **183**, 2063 (2012).
- ¹²M. A. Neumann, F. J. J. Leusen, and J. Kendrick, *Angew. Chem. Int. Ed.* **47**, 2427 (2008).
- ¹³A. M. Reilly, R. I. Cooper, C. S. Adjiman, S. Bhattacharya, A. D. Boese, J. G. Brandenburg, P. J. Bygrave, R. Bylsma, J. E. Campbell, R. Car, D. H. Case, R. Chadha, J. C. Cole, K. Cosburn, H. M. Cuppen, F. Curtis, G. M. Day, R. A. DiStasio Jr, A. Dzyabchenko, B. P. van Eijck, D. M. Elking, J. A. van den Ende, J. C. Facelli, M. B. Ferraro, L. Fusti-Molnar, C.-A. Gatsiou, T. S. Gee, R. de Gelder, L. M. Ghiringhelli, H. Goto, S. Grimme, R. Guo, D. W. M. Hofmann, J. Hoja, R. K. Hylton, L. Iuzzolino, W. Jankiewicz, D. T. de Jong, J. Kendrick, N. J. J. de Klerk, H.-Y. Ko, L. N. Kuleshova, X. Li, S. Lohani, F. J. J. Leusen, A. M. Lund, J. Lv, Y. Ma, N. Marom, A. E. Masunov, P. McCabe, D. P. McMahon, H. Meekes, M. P. Metz, A. J. Misquitta, S. Mohamed, B. Monserrat, R. J. Needs, M. A. Neumann, J. Nyman, S. Obata, H. Oberhofer, A. R. Oganov, A. M. Orendt, G. I. Pagola, C. C. Pantelides, C. J. Pickard, R. Podeszwa, L. S. Price, S. L. Price, A. Pulido, M. G. Read, K. Reuter, E. Schneider, C. Schober, G. P. Shields, P. Singh, I. J. Sugden, K. Szalewicz, C. R. Taylor, A. Tkatchenko, M. E. Tuckerman, F. Vacarro, M. Vasileiadis, A. Vazquez-Mayagoitia, L. Vogt, Y. Wang, R. E. Watson, G. A. de Wijs, J. Yang, Q. Zhu, and C. R. Groom, *Acta Cryst. B* **72**, 439 (2016).
- ¹⁴L. Iuzzolino, P. McCabe, S. L. Price, and J. G. Brandenburg, *Faraday Discuss.* **211**, 275 (2018).
- ¹⁵J. Hoja and A. Tkatchenko, *Faraday Discuss.* **211**, 253 (2018).
- ¹⁶J. Hoja, H. Y. Ko, M. A. Neumann, R. Car, R. A. Distasio, and A. Tkatchenko, *Sci. Adv.* **5** (2019).
- ¹⁷M. Mortazavi, J. Hoja, L. Aerts, L. Quéré, J. van de Streek, M. A. Neumann, and A. Tkatchenko, *Commun. Chem.* **2**, 1 (2019).
- ¹⁸S. R. Whittleton, A. Otero-de-la-Roza, and E. R. Johnson, *J. Chem. Theory Comput.* **13**, 441 (2017).
- ¹⁹S. R. Whittleton, A. Otero-de-la-Roza, and E. R. Johnson, *J. Chem. Theory Comput.* **13**, 5332 (2017).
- ²⁰L. M. LeBlanc and E. R. Johnson, *CrystEngComm* **21**, 5995 (2019).
- ²¹L. M. LeBlanc, A. Otero-de-la-Roza, and E. R. Johnson, *J. Chem. Theory Comput.* **14**, 2265 (2018).
- ²²C. R. Taylor, M. T. Mulvey, D. S. Perenyi, M. R. Probert, G. M. Day, and J. W. Steed, *J. Am. Chem. Soc.* **142**, 16668 (2020).
- ²³S. L. Price, M. Leslie, G. W. A. Welch, M. Habgood, L. S. Price, P. G. Karamertzanis, and G. M. Day, *Phys. Chem. Chem. Phys.* **12**, 8478 (2010).
- ²⁴B. Hourahine, B. Aradi, V. Blum, F. Bonafé, A. Buccheri, C. Camacho, C. Cevallos, M. Y. Deshayé, T. Dumitrică, A. Dominguez, S. Ehlert, M. Elstner, T. van der Heide, J. Hermann, S. Irle, J. J. Kranz, C. Köhler, T. Kowalczyk, T. Kubař, I. S. Lee, V. Lutsker, R. J. Maurer, S. K. Min, I. Mitchell, C. Negre, T. A. Neihaus, A. M. N. Niklasson, A. J. Page, A. Pecchia, G. Penazzi, M. P. Persson, J. Řezáč, C. G. Sánchez, M. Sternberg, M. Stöhr, F. Stuckenberg, A. Tkatchenko, V. W. z. Yu, and T. Frauenheim, *J. Chem. Phys.* **152**, 124101 (2020).
- ²⁵M. Kubillus, T. Kubař, M. Gaus, J. Řezáč, and M. Elstner, *J. Chem. Theory Comput.* **11**, 332 (2015).
- ²⁶R. Sure and S. Grimme, *J. Comput. Chem.* **34**, 1672 (2013).
- ²⁷M. Cutini, B. Civalleri, M. Corno, R. Orlando, J. G. Brandenburg, L. Maschio, and P. Ugliengo, *J. Chem. Theory Comput.* **12**, 3340 (2016).
- ²⁸J. Nyman and G. M. Day, *CrystEngComm* **17**, 5154 (2015).
- ²⁹J. Nyman and G. M. Day, *Phys. Chem. Chem. Phys.* **18**, 31132 (2016).
- ³⁰J. Nyman, O. S. Pundyke, and G. M. Day, *Phys. Chem. Chem. Phys.* **18**, 15828 (2016).
- ³¹Y. N. Heit and G. J. O. Beran, *Acta Cryst.* **B72**, 514 (2016).
- ³²C. Cook and G. J. O. Beran, *J. Chem. Phys.* **153**, 224105 (2020).
- ³³A. D. Becke, *J. Chem. Phys.* **85**, 7184 (1986).
- ³⁴J. P. Perdew, K. Burke, and M. Ernzerhof, *Phys. Rev. Lett.* **77**, 3865 (1996).
- ³⁵A. Otero-de-la-Roza and E. R. Johnson, *J. Chem. Phys.* **136**, 174109 (2012).
- ³⁶A. Otero-de-la-Roza and E. R. Johnson, *J. Chem. Phys.* **137**, 054103 (2012).
- ³⁷S. Baroni, S. de Gironcoli, A. D. Corso, and P. Giannozzi, *Rev. Mod. Phys.* **73**, 515 (2001).
- ³⁸H. J. Monkhorst and J. D. Pack, *Phys. Rev. B.* **13**, 5188 (1976).
- ³⁹P. Giannozzi, S. Baroni, N. Bonini, M. Calandra, R. Car, C. Cavazzoni, D. Ceresoli, G. L. Chiarotti,

- M. Cococcioni, I. Dabo, A. D. Corso, S. de Gironcoli, S. Fabris, G. Fratesi, R. Gebauer, U. Gerstmann, C. Gougoussis, A. Kokalj, M. Lazzeri, L. Martin-Samos, N. Marzari, F. Mauri, R. Mazzarello, S. Paolini, A. Pasquarello, L. Paulatto, C. Sbraccia, S. Scandolo, G. Sclauzero, A. P. Seitsonen, A. Smogunov, P. Umari, and R. M. Wentzcovitch, *J. Phys. Condens. Matter* **21**, 395502 (2009).
- ⁴⁰R. Dovesi, A. Erba, R. Orlando, C. M. Zicovich-Wilson, B. Civalleri, L. Maschio, M. Rérat, S. Casassa, J. Baima, S. Salustro, and B. Kirtman, *Wiley Interdiscip. Rev. Comput. Mol. Sci.* **8**, e1360 (2018).
- ⁴¹A. Togo and I. Tanaka, *Scr. Mater.* **108**, 1 (2015).
- ⁴²F. H. Allen, *Acta Cryst. B* **58**, 380 (2002), crystal structures can be obtained free of charge via http://www.ccdc.cam.ac.uk/data_request/cif.
- ⁴³A. D. Becke, *J. Chem. Phys.* **140**, 18A301 (2014).
- ⁴⁴P. E. Blöchl, *Phys. Rev. B* **50**, 17953 (1994).
- ⁴⁵E. R. Johnson, in *Non-covalent Interactions in Quantum Chemistry and Physics*, edited by A. Otero-de-la Roza and G. A. DiLabio (Elsevier, 2017) Chap. 5, pp. 169–194.
- ⁴⁶D. S. Coombes, S. L. Price, D. J. Willock, and M. Leslie, *J. Phys. Chem.* **100**, 7352 (1996).
- ⁴⁷D. E. Williams, *J. Comput. Chem.* **22**, 1154 (2001).
- ⁴⁸A. Abraha and D. E. William, *Inorg. Chem.* **38**, 4224 (1999).
- ⁴⁹A. J. Stone, *J. Chem. Theory Comput* **1**, 1128 (2005).
- ⁵⁰M. J. Frisch, G. W. Trucks, H. B. Schlegel, G. E. Scuseria, M. A. Robb, J. R. Cheeseman, G. Scalmani, V. Barone, B. Mennucci, G. A. Petersson, H. Nakatsuji, M. Caricato, X. Li, H. P. Hratchian, A. F. Izmaylov, J. Bloino, G. Zheng, J. L. Sonnenberg, M. Hada, M. Ehara, K. Toyota, R. Fukuda, J. Hasegawa, M. Ishida, T. Nakajima, Y. Honda, O. Kitao, H. Nakai, T. Vreven, J. A. Montgomery, Jr., J. E. Peralta, F. Ogliaro, M. Bearpark, J. J. Heyd, E. Brothers, K. N. Kudin, V. N. Staroverov, R. Kobayashi, J. Normand, K. Raghavachari, A. Rendell, J. C. Burant, S. S. Iyengar, J. Tomasi, M. Cossi, N. Rega, J. M. Millam, M. Klene, J. E. Knox, J. B. Cross, V. Bakken, C. Adamo, J. Jaramillo, R. Gomperts, R. E. Stratmann, O. Yazyev, A. J. Austin, R. Cammi, C. Pomelli, J. W. Ochterski, R. L. Martin, K. Morokuma, V. G. Zakrzewski, G. A. Voth, P. Salvador, J. J. Dannenberg, S. Dapprich, A. D. Daniels, Ö. Farkas, J. B. Foresman, J. V. Ortiz, J. Cioslowski, and D. J. Fox, “Gaussian 09 Revision E.01,” Gaussian Inc. Wallingford CT 2009.
- ⁵¹G. M. Day, S. L. Price, and M. Leslie, *J. Phys. Chem. B* **107**, 10919 (2003).
- ⁵²P. Sacchi, M. Lusi, A. J. Cruz-Cabeza, E. Nauha, and J. Bernstein, *CrystEngComm* **22**, 7170 (2020).
- ⁵³R. Sure and S. Grimme, *J. Chem. Theory Comput.* **11**, 3785 (2015).